DAΦNE TECHNICAL NOTE
INFN - LNF, Accelerator Division

Frascati, March 22, 2004
Note: **L-35**

HARD-EDGE MODEL OF THE DAΦNE WIGGLERS

G. Benedetti, C. Milardi, M. Preger, P. Raimondi

Introduction

The modified wiggler magnets of the Main Rings have been modeled as a *2 m* long sequence of hard-edge dipoles alternated with drift sections describing the behaviour of the magnet for the linear beam optics. Two additional thin lenses per pole positioned at the edges reproduce the non-linear terms of the field. The physical parameters of the model are based on the measurement of the field B_y versus the position (x,z) in the horizontal midplane of the central pole and on the two terminal poles, which has been taken on the modified wiggler on August and September 2003 [1]. The model is used for simulations of the Main Ring beam optics with the MAD program.

1. Linear properties

For the proper linear modeling of wiggler magnets two conditions require to be fulfilled. The deflection angle and the length of each modeled pole must be the same of the actual trajectory. Similarly the edge focusing described in the model (the *fint* parameter used by the MAD modeling code) must be the same felt by a particle travelling around the trajectory. The corrections to the linear optics due to the wiggling trajectory through multipole field components is considered in a following step and added to the model as thin lenses as described in the second section of this note.

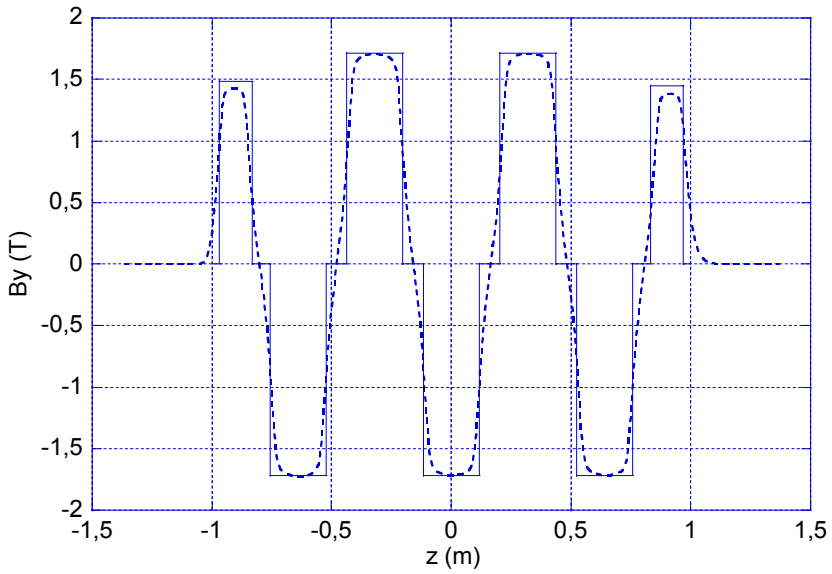

Figure 1 – The wiggler field along the longitudinal z axis: the dashed line is the measured field and the full line the hard-edge model.

The trajectory of the nominal particle

The first step is the calculation of the trajectory of the nominal particle along the whole wiggler. The magnetic field on the horizontal midplane ($y = 0$), where the trajectory lies, has only the vertical component $B_y(x,0,z)$, while $B_{x,z}(x,0,z) = 0$, therefore a charged particle undergoes the Lorentz force according to:

$$\ddot{x} = -\frac{e}{p_0}\dot{z}B_y(x,z)$$
$$\ddot{z} = \frac{e}{p_0}\dot{x}B_y(x,z)$$

The wiggle in Figure 2 is the trajectory along the magnet, for the nominal particle launched at the entrance to the pole A with $x = -12.5$ *mm* and $x' = 0$ *rad*, obtained by integration of the equations above performed as described in Appendix A of this note.

The length of the wiggling path comes out to be *6.62 mm* longer than the longitudinal straight line along the axis.

Once the amplitude, the deflection angle and the length of the trajectory are known, the wiggler can be modeled pole by pole. Each pole is represented by a single parallel-end hard-edge dipole with length L_h (Figure 1) embedded in two drift sections with length L_d: the total length of the pole $L_p = L_h + 2L_d$ is fixed equal to the nominal particle path length integrated along the pole. The modeling problem consists in the choice of L_h.

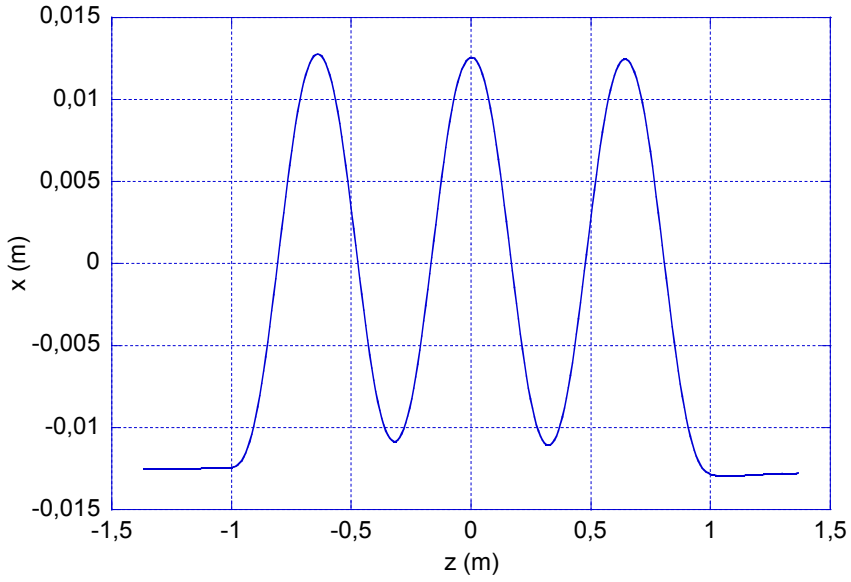

Figure 2 – The wiggling trajectory: the particle launched from the terminal pole A.

Inner Poles

In the model the inner poles are assumed to be equal among them and the physical parameters are obtained from the measurements performed on the central pole. The deflection angle of the

central pole comes out to be $\theta_C = \pm 0.2375\ rad$ and the entrance and exit angles are half the deflection angle: $e_1 = e_2 = \theta/2$.

Since the dipole has parallel ends, in the horizontal plane there is no focusing effect and the horizontal transport matrix does not depend on L_h but only on the total pole length L_p that is fixed. Therefore the dipole length and the edge focusing parameter *fint* have been chosen in order to match the vertical transfer matrix of the single pole calculated from the measured field map as described in Appendix B. The obtained values are $L_h = 0.2355\ m$ and $fint = 0.315$.

End Poles

One of the end poles (B type or "Right") has a strong sextupole field index useful to improve the dynamic aperture: as a consequence the poles A and B, which are powered by the same supply, have slightly different field integrals and different deflection angles between them. The supplied current is such that the field integral along the wiggler axis vanishes ($\int B_y\, dz = 0$). The deflection angle of the right pole is $\theta_B = -0.1196\ rad$ and the left one $\theta_A = -0.1167\ rad$. The entrance and exit angles are: $e_1 = 0$, $e_2 = \theta_{A,B}$.

The end dipole length and the *fint* parameter chosen with the same procedure followed for the central poles are $L_h = 0.1368\ m$ and $fint = 0.213$.

2. Linear and non-linear field perturbations as thin lenses

Finite horizontal pole width in a wiggler magnet creates a roll-off in $B_y(x)$ which generates linear and non-linear perturbations to the particle dynamics [2, 3]. The Figure 3 shows $B_y(x)$ at the wiggler centre fitted from measurements: the $14\ cm$ pole width results in the field rolling off quickly at $\pm 50\ mm$.

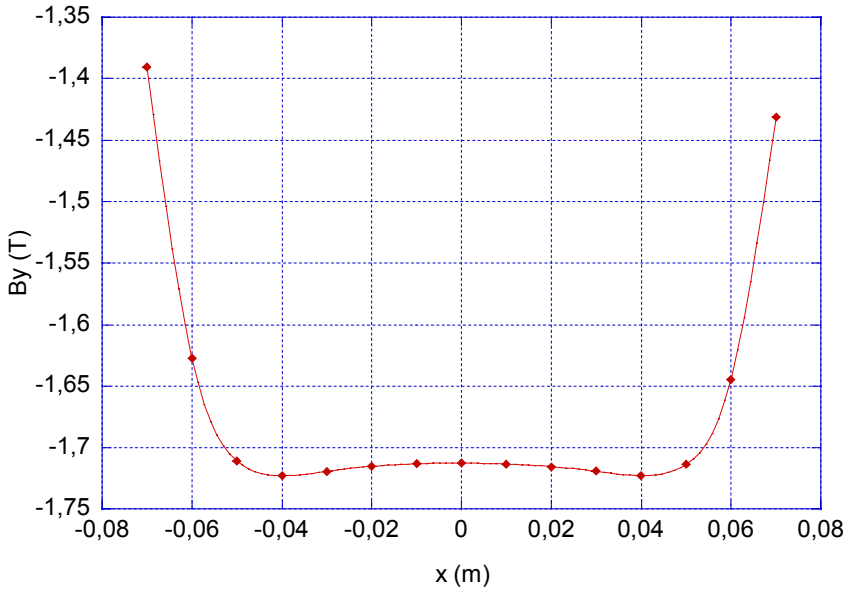

Figure 3 – Transverse field roll-off at the centre of the wiggler.

The transverse polynomial expansion of the field [1] shows up a small but not negligible sextupole term and higher multipoles that give linear and non-linear perturbations to both the horizontal and the vertical motion around the trajectory. All these effects are taken in account in the model embedding each dipole in two thin lenses with integrated gradients along the trajectory:

$K1 = (1/B\rho) \int dB_y/dx \; ds = (1/B\rho) \int (\partial B_y/\partial x + \partial^2 B_y/\partial x^2 \cdot x + \partial^3 B_y/\partial x^3 \cdot x^2/2 + \partial^4 B_y/\partial x^4 \cdot x^3/6)\, dz$;

$K2 = (1/B\rho) \int d^2 B_y/dx^2 \, ds = (1/B\rho) \int (\partial^2 B_y/\partial x^2 + \partial^3 B_y/\partial x^3 \cdot x + \partial^4 B_y/\partial x^4 \cdot x^2/2)\, dz$;

$K3 = (1/B\rho) \int d^3 B_y/dx^3 \, ds = (1/B\rho) \int (\partial^3 B_y/\partial x^3 + \partial^4 B_y/\partial x^4 \cdot x)\, dz$;

$K4 = (1/B\rho) \int d^4 B_y/dx^4 \, ds = (1/B\rho) \int \partial^4 B_y/\partial x^4 \, dz$.

The *K1* coefficients are chosen fitting the single pole transfer matrices (Appendix B), while *K2*, *K3* and *K4* come from the magnetic measurements fit ([1] Table I). In the model of the inner poles the average value among the five poles is taken for each *Kn* coefficient. Only in the end pole B, where the sextupole term is strong and quite constant (see [1] Fig. 32), the sextupole gradient *K2* is spread out along the whole dipole.

	End Pole A	Inner Poles	End Pole B
L_h (m)	0.1368	0.2355	0.1368
L_p (m)	0.20	0.32	0.20
Bend Angle (rad)	0.1167	0.2375	0.1196
fint	0.384	0.317	0.384
K1 (m^{-1})	0.0	-0.0022	0.0260
K2 (m^{-2})	0.23	±0.78	34.4
K3 (m^{-3})	23.0	-34.4	15.0
K4 (m^{-4})	-0.0025	±0.0045	-0.0014

Table 1 – The parameters of the model.

3. Results of the MAD model

The model is able to reproduce with very good accuracy the linear matrix elements calculated from measurements ($\Delta m \approx 10^{-4}$). After the whole map of the field on the midplane was measured (October 2003), the *fint* parameters have been further finely readjusted in order to match the whole wiggler transfer matrix obtained from the magnetic measurements [1] and are reported below.

The central pole matrix:

```
1.0007      0.3189      0.0000      0.0000
0.0044      1.0007      0.0000      0.0000
0.0000      0.0000      0.9647      0.3184
0.0000      0.0000     -0.2174      0.9647
```

The end pole A matrix (travelling towards the inside of the wiggler):

```
0.9928      0.2004      0.0000      0.0000
0.0000      1.0072      0.0000      0.0000
0.0000      0.0000      0.9981      0.2000
0.0000      0.0000     -0.0822      0.9853
```

The end pole B matrix (travelling towards the inside of the wiggler):

```
0.9989      0.2006      0.0000      0.0000
0.0520      1.0115      0.0000      0.0000
0.0000      0.0000      0.9923      0.1997
0.0000      0.0000     -0.1307      0.9813
```

The whole wiggler from A to B:

```
1.1230        2.0465        0.0000        0.0000
0.0745        1.0263        0.0000        0.0000
0.0000        0.0000       -0.0851        1.1980
0.0000        0.0000       -0.8327       -0.0266
```

The whole wiggler from B to A:

```
1.0263        2.0465        0.0000        0.0000
0.0745        1.1230        0.0000        0.0000
0.0000        0.0000       -0.0266        1.1980
0.0000        0.0000       -0.8328       -0.0851
```

Notice that due to the asymmetry between the pole A and B, exchanging the direction of motion in the case of the whole matrix, diagonal elements are exchanged in the horizontal and vertical blocks, while off diagonal ones are unchanged. The total matrix in reference [1] is calculated along a length of *2.2165 m* while the matrices above corresponds to a *2 m* long modeled wiggler

4. Final remarks on the model

Two important remarks on the accuracy of the model: the first about the dependence of the wiggler optics on the orbit and the second finally on the contribution to the radiation integral.

As seen in Section 2 the terminal pole B has a strong sextupole, which generates linear focusing depending on the horizontal trajectory. A horizontal displacement of the trajectory of the order of the r.m.s. orbit value changes the effective *K1* coefficient by about $\Delta K1 \approx K2\ \Delta x = 4.7\ m^{-2}$ $1.5\ mm \approx 0.007\ m^{-1}$. This variation affects mainly the horizontal dispersion function of the ring, which has its maximum right near the wigglers. The model is indeed corrected adding a further thin lens with *K1* adjusted fitting the measured dispersion.

The curvature of the poles should reproduce the wiggler contribution to quantum excitation and damping of the beam emittance and beam energy spread. The quantum excitation is in first approximation proportional to the third power of the curvature (the radiation integrals $I_3$and I_5):

$$\sum_{poles} \frac{L_h}{\rho^3} = 1.381\ \mathrm{m}^{-2}$$

$$\frac{1}{(B\rho)^3} \int_{wiggl} B^3 ds = 1.135\ \mathrm{m}^{-2}$$

with a mismatch between model and real wiggler of the 17 % that must be considered.

Appendix A: calculation of the Trajectory

On the midplane of the magnet, where the particle trajectory lies, the field is always vertical. In the reference system in Figure 6 the particle velocity is: $\dot{\mathbf{r}} = c\,\mathbf{u}_s$ and the magnetic field: $\mathbf{B}(x,z) = B_y(x,z)\,\mathbf{u}_y$.

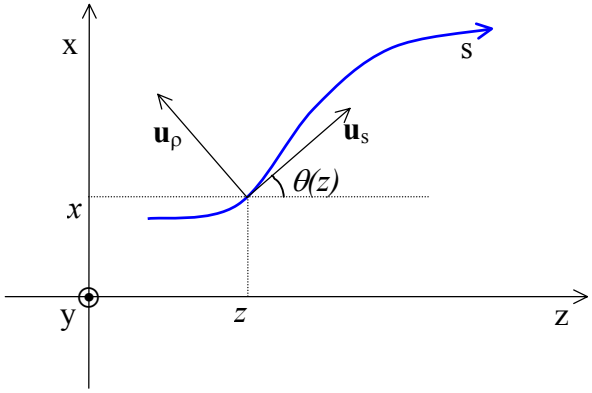

Figure 6 – The global and the local coordinate systems along the trajectory.

Therefore the equation of motion $\gamma m\,\ddot{\mathbf{r}} = e\,\dot{\mathbf{r}} \times \mathbf{B}$ becomes:

$$\ddot{\mathbf{r}} = \frac{e}{\gamma m} cB_y \mathbf{u}_s \times \mathbf{u}_y = -\frac{e}{\gamma m} cB_y \mathbf{u}_\rho = -\frac{e}{p_0} c^2 B_y (\cos\theta\,\mathbf{u}_x - \sin\theta\,\mathbf{u}_z);$$

which is the system:

$$\ddot{x} = -\frac{e}{p_0} c^2 B_y(x,z)\cos\theta$$
$$\ddot{z} = \frac{e}{p_0} c^2 B_y(x,z)\sin\theta$$

where $tg\,\theta = dx/dz$.

The derivatives in the system above are done with respect to the time variable t, while the magnetic field $B_y(x,z)$ is known from measurement as a function of the position in the midplane as well as $\theta(z)$ is expressed as a function of the longitudinal position z. Therefore z is the most suitable variable for numerical integration. Considering $c\,dt = ds = [1+(dx/dz)^2]^{1/2}\,dz$, the second derivative is expressed according to:

$$\ddot{x} \equiv \frac{d^2x}{dt^2} = c^2 \frac{d^2x}{ds^2} = c^2 \frac{1}{\sqrt{1+\left(\frac{dx}{dz}\right)^2}} \frac{d}{dz}\left[\frac{1}{\sqrt{1+\left(\frac{dx}{dz}\right)^2}} \frac{dx}{dz}\right] = c^2 \frac{1}{\left(1+\left(\frac{dx}{dz}\right)^2\right)^2} \frac{d^2x}{dz^2} = c^2 \cos^4\theta \frac{d^2x}{dz^2}$$

and after the variable change the trajectory equation becomes:

$$\cos^3\theta(z)\frac{d^2x}{dz^2} = -\frac{e}{p_0}B_y(x,z)$$

and eventually:

$$\frac{d^2x}{dz^2} = -\frac{1}{B\rho}\left[1+\left(\frac{dx}{dz}\right)^2\right]^{\frac{3}{2}}B_y(x,z)$$

This differential equation can be numerically integrated from the field measurements table with a recursive algorithm with start path $x(z) = 0$. The spacing between points in the data table is *1 cm*, both longitudinally and horizontally. The field $B_y(z)$ is first fitted with a cubic *spline* curve (a series of cubic polynomials connected together) and then integrated with *1 mm* longitudinal steps. The integration converges after few iterations (2-3) since within the ± 12.5 *mm* horizontal range, where the trajectory oscillates, B_y has little and smooth variations and dx/dz is small ($\Delta B/B < 2\cdot 10^{-3}$ and $dx/dz < 0.12$).

Once the trajectory is known, the path length is calculated from:

$$L_{traj} = \int_{wiggler} ds = \int_{wiggler}\sqrt{1+\left(\tfrac{dx}{dz}\right)^2}\,dz\,.$$

Appendix B: calculation of the Linear Transfer Matrix

Once the wiggling trajectory was known, the transfer matrix of each single pole has been calculated from the table of the field measurements.

Linear Transfer Matrix

On the horizontal midplane of each pole the field is everywhere vertical (Figure 7) therefore in a parallel end dipole (neglecting at the moment the finite horizontal width of the magnet) there is no focusing effect on the horizontal plane.

The scenario changes for a particle displaced vertically. In this case it undergoes the longitudinal component B_z of the field in the fringing region, which is responsible of the edge vertical focusing in a dipole[1]. Launching a particle with *(y, y') = (1, 0)* and *(y, y') = (0, 1)*, the values of the position *y* and the divergence *y'* at the end of the pole are the columns of the vertical transfer matrix and the physical problem consists in the tracking of the particle around the trajectory previously calculated. The vertical equation of motion is (see Figure 7):

$$\ddot{y} = \frac{ec}{p_0}\left(\dot{\mathbf{r}} \times \mathbf{B}\right)_y = \frac{ec^2}{p_0} B_z \sin\theta$$

deriving with respect to z:

$$\cos^4\theta \frac{d^2 y}{dz^2} = \frac{e}{p_0} B_z \sin\theta$$

Figure 7 – Projections of a parallel-end dipole showing the fringe field.

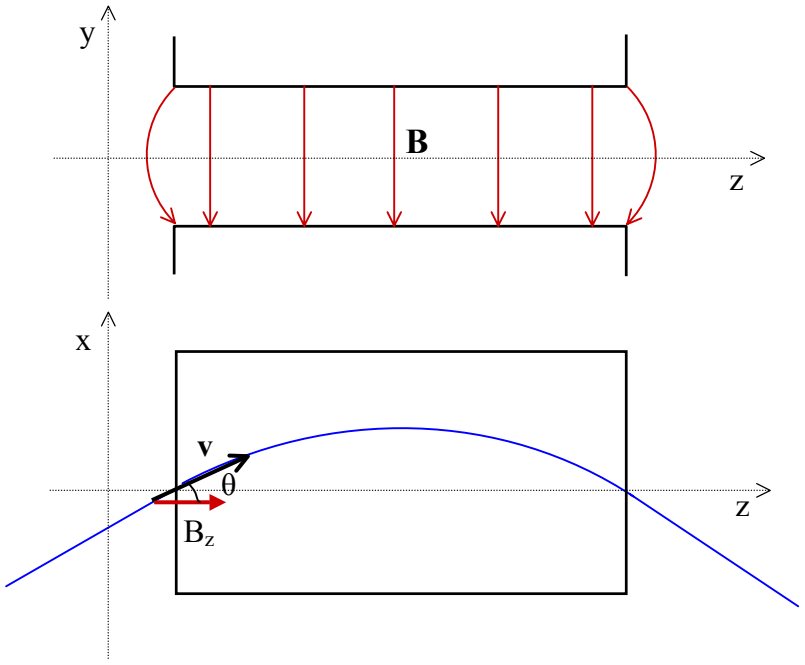

[1] Further considerations are reported in the slides presented in the optics internal meeting held on 26 June 2003, available on: *www.lnf.infn.it/acceleratori/dafne/report/WigglerModel.pdf*

and eventually:

$$\frac{d^2y}{dz^2} = \frac{1}{B\rho}\left(1+\left(\frac{dx}{dz}\right)^2\right)^{\frac{3}{2}} \frac{dx}{dz} B_z(x,z)$$

where *dx/dz* is the derivative of the horizontal wiggling trajectory.

For linear modeling the field components at position *y* can be estimated expanding the magnetic field to first order around the midplane (*y = 0)*, where the field is known. Using also Maxwell's equations:

$$B_x(x,y,z) = y\left(\frac{\partial B_x}{\partial y}\right)_{y=0} = y\left(\frac{\partial B_y}{\partial x}\right)_{y=0}$$

$$B_y(x,y,z) = B(x,0,z) + y\left(\frac{\partial B_y}{\partial y}\right)_{y=0} = B(x,0,z) - y\left(\frac{\partial B_x}{\partial x} + \frac{\partial B_z}{\partial z}\right)_{y=0} = B(x,0,z)$$

$$B_z(x,y,z) = y\left(\frac{\partial B_z}{\partial y}\right)_{y=0} = y\left(\frac{\partial B_y}{\partial z}\right)_{y=0}$$

The behaviour of $B_y(x,z)$ has been measured and fitted and the vertical trajectory can be numerically integrated with the same procedure followed for the wiggling trajectory. The dipole lengths and the *fint* parameters are then fixed pole by pole fitting the matrix elements by using the matching commands of the MAD program.

Linear perturbations of the Transfer Matrix

The final step is to consider the linear corrections to transfer matrix integrating the complete equation of motion that takes in account the horizontal roll off of the field, which generates multipole terms. In the model this is realized adding thin lenses at the dipole edges, whose integrated gradient values *K1* have been found matching again the corrected transfer matrix calculated from the equation of motion:

$$\ddot{y} = \frac{ec}{p_0}\left(\dot{\mathbf{r}} \times \mathbf{B}\right)_y = \frac{ec^2}{p_0}\left(B_z \sin\theta - B_x \cos\theta\right)$$

which gives:

$$\frac{d^2y}{dz^2} = \frac{1}{B\rho}\left(1+\left(\frac{dx}{dz}\right)^2\right)^{\frac{3}{2}}\left(\frac{dx}{dz} B_z(x,z) - B_x(x,z)\right)$$

The integrated vertical trajectories through the single poles are shown in Figures 4 and 5

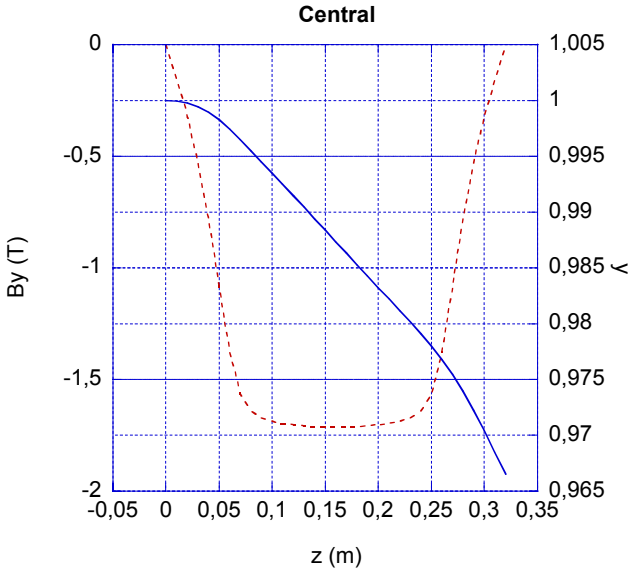

Figure 4 – The vertical trajectory (full line) in the central pole entering in the pole with (y, y') = (1, 0); the dashed line is the magnetic field.

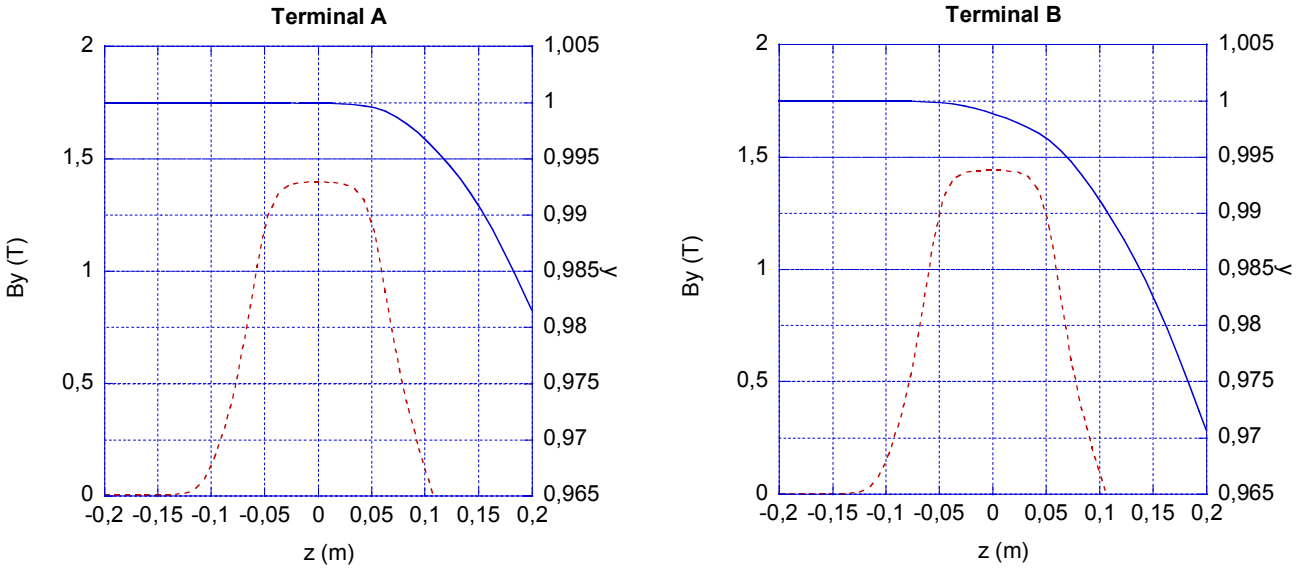

Figure 5 – The vertical trajectory (full line) in the terminal poles starting with (y, y') = (1, 0): the terminal B has an extra-focusing term due to the sextupole; the dashed line is the magnetic field.

References

[1] – M. Preger et Al., *The Modified Wiggler Model of the DAFNE Main Rings*, DAFNE Technical Note MM-34 (2004)

[2] – M. Bassetti, C. Biscari, M. Preger, *Optical Characteristics of the DAFNE Wiggler*, DAFNE Technical Note G-27 (1994)

[3] – J. Safranek et Al., *Non Linear Dynamics in a SPEAR Wiggler*, Phys. Rev. Vol. 5, 010701 (2002)